

AD-A210 770

Picosecond Carrier Dynamics Near the Gallium Arsenide Surface

D. C. MARVIN, S. M. BECK, and J. E. WESSEL
Chemistry and Physics Laboratory
Laboratory Operations
Development Group

and

J. G. ROLLINS
Electronics and Optics Division
Engineering Group
The Aerospace Corporation
El Segundo, CA 90245

28 March 1989

Prepared for

SPACE SYSTEMS DIVISION
AIR FORCE SYSTEMS COMMAND
Los Angeles Air Force Base
P.O. Box 92960
Los Angeles, CA 90009-2960

APPROVED FOR PUBLIC RELEASE;
DISTRIBUTION UNLIMITED


DTIC
ELECTE
AUG 01 1989
S B D

This report was submitted by The Aerospace Corporation, El Segundo, CA 90245, under Contract No. F04701-85-C-0086-P00016 with the Space Systems Division, P.O. Box 92960, Los Angeles, CA 90009-2960. It was reviewed and approved for The Aerospace Corporation by S. Feuerstein, Director, Chemistry and Physics Laboratory.

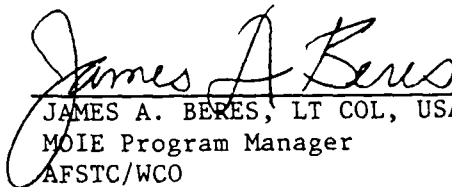
Lt Stephen A. Way was the Air Force project officer for the Mission-Oriented Investigation and Experimentation (MOIE) program.

This report has been reviewed by the Public Affairs Office (PAS) and is releasable to the National Technical Information Service (NTIS). At NTIS, it will be available to the general public, including foreign nationals.

This technical report has been reviewed and is approved for publication. Publication of this report does not constitute Air Force approval of the report's findings or conclusions. It is published only for the exchange and stimulation of ideas.



STEPHEN A. WAY, LT, USAF
MOIE Project Monitor
AFSTC/WCO



JAMES A. BERES, LT COL, USAF
MOIE Program Manager
AFSTC/WCO

UNCLASSIFIED

SECURITY CLASSIFICATION OF THIS PAGE

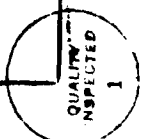
REPORT DOCUMENTATION PAGE

1a. REPORT SECURITY CLASSIFICATION Unclassified			1b. RESTRICTIVE MARKINGS		
2a. SECURITY CLASSIFICATION AUTHORITY			3. DISTRIBUTION/AVAILABILITY OF REPORT Approved for public release; distribution unlimited.		
2b. DECLASSIFICATION DOWNGRADING SCHEDULE					
4. PERFORMING ORGANIZATION REPORT NUMBER(S) TR-0086A(2945-06)-1			5. MONITORING ORGANIZATION REPORT NUMBER(S) SD-TR-89-27		
6a. NAME OF PERFORMING ORGANIZATION The Aerospace Corporation Laboratory Operations		6b. OFFICE SYMBOL (If applicable)	7a. NAME OF MONITORING ORGANIZATION Space Systems Division		
6c. ADDRESS (City, State, and ZIP Code) El Segundo, CA 90245			7b. ADDRESS (City, State, and ZIP Code) Los Angeles Air Force Base Los Angeles, CA 90009-2960		
8a. NAME OF FUNDING/SPONSORING ORGANIZATION		8b. OFFICE SYMBOL (If applicable)	9. PROCUREMENT INSTRUMENT IDENTIFICATION NUMBER FO4701-85-C-0086-P00016		
8c. ADDRESS (City, State, and ZIP Code)			10. SOURCE OF FUNDING NUMBERS		
			PROGRAM ELEMENT NO	PROJECT NO	TASK NO
			WORK UNIT ACCESSION NO.		
11. TITLE (Include Security Classification) Picosecond Carrier Dynamics Near the Gallium Arsenide Surface					
12. PERSONAL AUTHOR(S) Marvin, Dean C.; Beck, Steven M.; Wessel, John E.; and Rollins, J. Gregory					
13a. TYPE OF REPORT		13b. TIME COVERED FROM _____ TO _____		14. DATE OF REPORT (Year, Month, Day) 1989 March 28	
				15. PAGE COUNT 30	
16. SUPPLEMENTARY NOTATION					
17. COSATI CODES			18. SUBJECT TERMS (Continue on reverse if necessary and identify by block number)		
FIELD	GROUP	SUB-GROUP	Gallium arsenide; Picosecond reflectivity		
			Carrier dynamics; Surface recombination		
19. ABSTRACT (Continue on reverse if necessary and identify by block number)					
<p>Numerical modeling procedures were applied to experimental data from picosecond transient-reflectivity experiments in order to characterize carrier dynamics near the GaAs surface. A wide range of surfaces was studied. The results provide an excellent description of carrier dynamics for (100) surfaces of intrinsic, n-doped, and Cr-doped material. An analytical model, including ambipolar diffusion, bulk recombination, and surface recombination, describes results for the washed material. Surface charge present in unwashed material necessitated use of a more complex numerical model that treats electrons and holes separately. This provided a good description of reflectivity kinetics for the above sample types. The relationship of the new work to prior related work is reviewed.</p>					
20. DISTRIBUTION/AVAILABILITY OF ABSTRACT			21. ABSTRACT SECURITY CLASSIFICATION		
<input checked="" type="checkbox"/> UNCLASSIFIED/UNLIMITED <input type="checkbox"/> SAME AS RPT. <input type="checkbox"/> DTIC USERS			Unclassified		
22a. NAME OF RESPONSIBLE INDIVIDUAL			22b. TELEPHONE (Include Area Code)		22c. OFFICE SYMBOL

CONTENTS

I	INTRODUCTION.....	3
II.	EXPERIMENTAL.....	5
III.	RESULTS.....	7
IV.	DISCUSSION.....	21
V.	CONCLUSION.....	25
	REFERENCES.....	27

Accession For	
NTIS GRA&I	<input checked="" type="checkbox"/>
DTIC TAB	<input type="checkbox"/>
Unannounced	<input type="checkbox"/>
Justification	
By _____	
Distribution/	
Availability Codes	
Dist	Avail and/or Special
A-1	



FIGURES

1.	Schematic diagram of the experimental apparatus.....	6
2.	Picosecond transient reflectivity decay recorded for unwashed n-type GaAs nominally doped with silicon.....	8
3.	Picosecond transient reflectivity decays recorded for unwashed (111) and (-1,-1,-1) GaAs nominally doped with silicon, same wafer.....	9
4.	Picosecond transient reflectivity decay recorded for unwashed p-doped GaAs doped with Zn to $8 \times 10^{18} \text{ cm}^{-3}$	10
5.	Picosecond transient reflectivity decay recorded for photowashed GaAs with fit by ambipolar diffusion model.....	13
6.	Comparison of the measured reflectivity decay for typical unwashed n-type GaAs and the best fitting achieved using the ambipolar diffusion model.....	15
7.	Calculation of best fit by the PISCES calculation to data for photowashed n-type GaAs, using hole density as the time dependent variable.....	17
8.	Time dependence of electron density predicted for positive surface charge is compared with the observed decay from photowashed n-type GaAs.....	18
9.	Predicted time dependence of hole density decay with surface charge and surface recombination velocity adjusted for an optimum fit to data for typical unwashed n-type GaAs.....	19
10.	Predicted time dependence of electron density with surface charge and surface recombination velocity adjusted for an optimum fit to data for typical unwashed n-type GaAs.....	20

I. INTRODUCTION

Native GaAs (100) surfaces are subject to severe Fermi level pinning effects, attributed to surface states¹. Transient-reflectivity experiments can probe charge carrier transport processes in the region where they are strongly influenced by the surface. Most of the prior studies² of photoreflexion spectroscopy were performed on time scales of microseconds and longer, in which photogenerated carriers modulate reflectivity through the Franz-Keldysh effect. Thus, the experiments yield information on the static surface fields. The slow techniques do not necessarily measure the same processes as those observed on the picosecond time scale. Recently, we reported³ studies of picosecond transient reflectivity for GaAs surfaces prepared by a photowashing technique. The results suggested that surfaces can be prepared substantially free of band bending and that the picosecond transient-reflectivity technique can quantitatively measure surface recombination velocities for these samples. The studies also demonstrated convincingly that the simple model for recombination kinetics, based on ambipolar diffusion, bulk recombination, and surface recombination, does not account for the complex, rapid decay observed for ordinary untreated and normal etched GaAs surfaces. This implies that surface recombination velocities calculated for this type of sample using prior flat band models are highly inaccurate.

The objective of this study is to demonstrate that the complex carrier dynamics revealed by the picosecond experiments can be modeled quantitatively for samples characterized by large surface fields. A sophisticated computer code was used to simulate carrier dynamics that match the high quality picosecond data now available. Calculations are based on the PISCES computer code⁴ described in detail below, which self-consistently incorporates the effect of time-dependent internal electric fields and two-dimensional diffusion. The computer code was modified to include photoinjection of charge carriers. Data are fit by adjusting the unknown values for surface recombination velocity and initial surface charge density. We show that the

results converge on those provided by the analytical model for flat band conditions, and they also provide an excellent fit for the more complex decays observed for typical pinned surfaces.

Most prior picosecond optical studies^{5,6} neglected the problem of surface fields, and the experiments generally employed injected carrier densities large enough to induce nonlinear processes, such as Auger recombination. Our measurements are performed at substantially lower injected charge carrier densities, such that nonlinear recombination is not evident. In some of these studies⁴, transient grating techniques were employed, where lateral diffusion processes are emphasized because of the fine grating period. The reflection technique employed used here is relatively insensitive to diffusion in the surface plane.

Several studies^{7,8} have addressed the effects of photowashing on GaAs, as measured by techniques such as photoluminescence. In these studies luminescence was used on a steady state basis and did not provide direct dynamic information. Radiative recombination is presumably reduced in the region of surface fields because charge carriers are rapidly separated by the field. Thus, increases in luminescence yield due to processing are attributed to decreases in surface band bending. By this means, and by capacitance/voltage measurements on metal-insulator-semiconductor (MIS) structures, Woodall and coworkers⁷ initially established that photowashing can change the surface properties of GaAs. Our studies are more direct in that they probe charge-carrier-related properties quite near the unmodified surface. Based on the treatment of surface reflectivity by Aspnes and Froya⁹, the reflectivity signal arises from a characteristic depth estimated to be 10^{-6} cm, for an absorption coefficient of 10^{-4} cm⁻¹ at room temperature (i.e., GaAs at 820 nm). Thus, sampling occurs directly at the surface, and does not require convolution across the beam penetration depth. The actual physical mechanism responsible for reflectivity changes is not entirely clear at present. It is briefly reviewed in the Discussion section.

II. EXPERIMENTAL

The experimental apparatus is described in Fig. 1. A synchronously pumped picosecond dye laser system provided pump and probe pulse trains of low fluence. The pump pulses were typically above bandgap, at about 820 nm (the room temperature bandgap of GaAs is near 1.43 eV, corresponding to 867 nm), with a fluence of approximately 2×10^{-5} J/cm². The pulse duration was measured to be near 10 ps, and the repetition rate was 228 MHz. The pump beam was electro-optically modulated at 14 MHz. A second dye laser provided a probe pulse train, characterized by fluences an order of magnitude less than the pump, and by wavelengths varying from above to below bandgap, depending on the measurement. Both pump and probe were incident at 45°, and the probe was focused to a slightly smaller spot size than the pump. The probe beam passed through an optical delay line that was scanned over the range -20 to +400 ps delay. The reflected probe beam was separated from the pump beam by a monochromator, and detected by a silicon photodiode. Signals imposed on the probe beam were detected at the 14-MHz modulation frequency using a high frequency lock-in amplifier. The output was digitized and signal averaged, as a function of delay time between pump and probe pulses. In all cases, the reflectivity decayed approximately to background levels between laser pulses. There was no evidence of heating effects or of sample damage in the reported experiments. Only in the case of photowashed samples did signals change with time. This was somewhat dependent on pump beam irradiation conditions. Larger changes, associated with atmospheric surface chemistry, occurred on time scales varying from 10 minutes to a day following washing.

Photowashing was performed with the sample mounted in the picosecond reflectivity apparatus. A stream of deionized distilled water was passed over the surface while the sample was irradiated with about 1 W cm⁻² output from the 514-nm argon ion laser beam. Typically, this was continued for about 5 min, then the sample was dried with a stream of ultrapure nitrogen. These conditions resulted in the slowest, most uniform decay curves observed, and also with the largest amplitude reflectivity changes. More extensive washing generally resulted in degraded signals.

Samples were acquired from a variety of sources. Commercial intrinsic, n-doped, and p-doped (100) and commercial n-doped (111) GaAs wafers were examined, as received from manufacturers, after bromine-methanol etch procedures were performed, and after photowashing treatment.

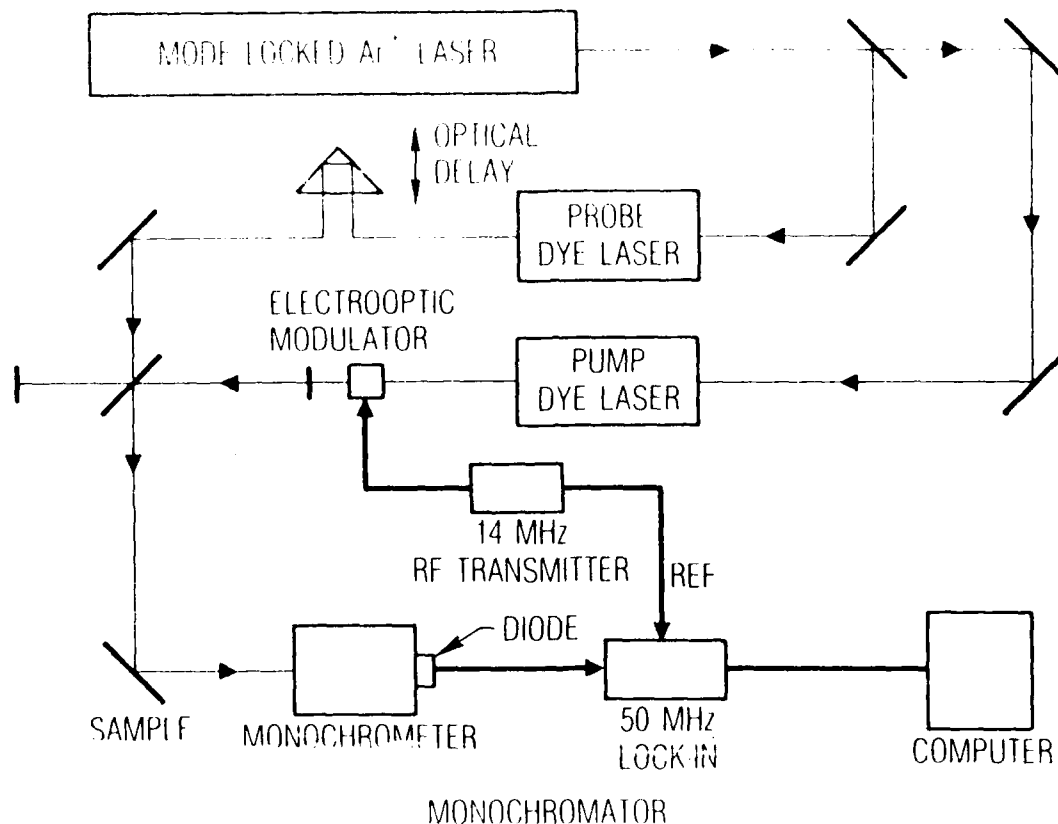


Fig. 1. Schematic diagram of the experimental apparatus

III. RESULTS

For above-bandgap probe energies, transient reflectivity signals are generally characterized by a rapid increase in reflectivity, followed by decay, spanning periods from 50 to 400 ps, depending on the surface condition. Signal amplitudes and functional forms are highly dependent on sample type, orientation, and processing conditions. Photowashed (100) surfaces of intrinsic, n-doped, and Cr-doped GaAs produced signals with the slowest decays and highest amplitudes. In addition, signals from these samples were highly uniform from sample to sample. Typical examples of transient reflectivity for as-received samples are shown in Figs. 2 and 3. It should be noted that, for some samples, the sign of the reflectivity change reversed between front and back surfaces, particularly for polar (111) material (Fig. 3). Typical signals from p-type material, shown in Fig. 4, were notably distinct from and were of opposite sign to those typical of n-type material. This difference was observed for both as-received and photowashed samples.

Response was highly uniform for photowashed intrinsic, Cr-doped, and n-type samples from diverse sources. Maximum amplitude signals were obtained for washes of about 5-min duration. Under exposure to normal atmospheric conditions following photowashing, similar signals were observed for consecutive measurements, provided the time between measurements was less than several hours. Signal levels declined somewhat for longer delays, and accelerated decline in signals was correlated with less stringent washing procedures. For several samples, measurements were made at many positions on the sample surface, and the results were essentially identical. The same was observed for unprocessed, nominally clean samples.

Figure 2 displays a typical decay curve recorded for n-type (100) GaAs as-received surfaces. The signal is essentially biexponential, with approximate time constants of 80 and 180 ps. The relative amplitudes and time constants of the fast and slow components varied appreciably, although the general form of the decay was relatively consistent. The signal risetime was

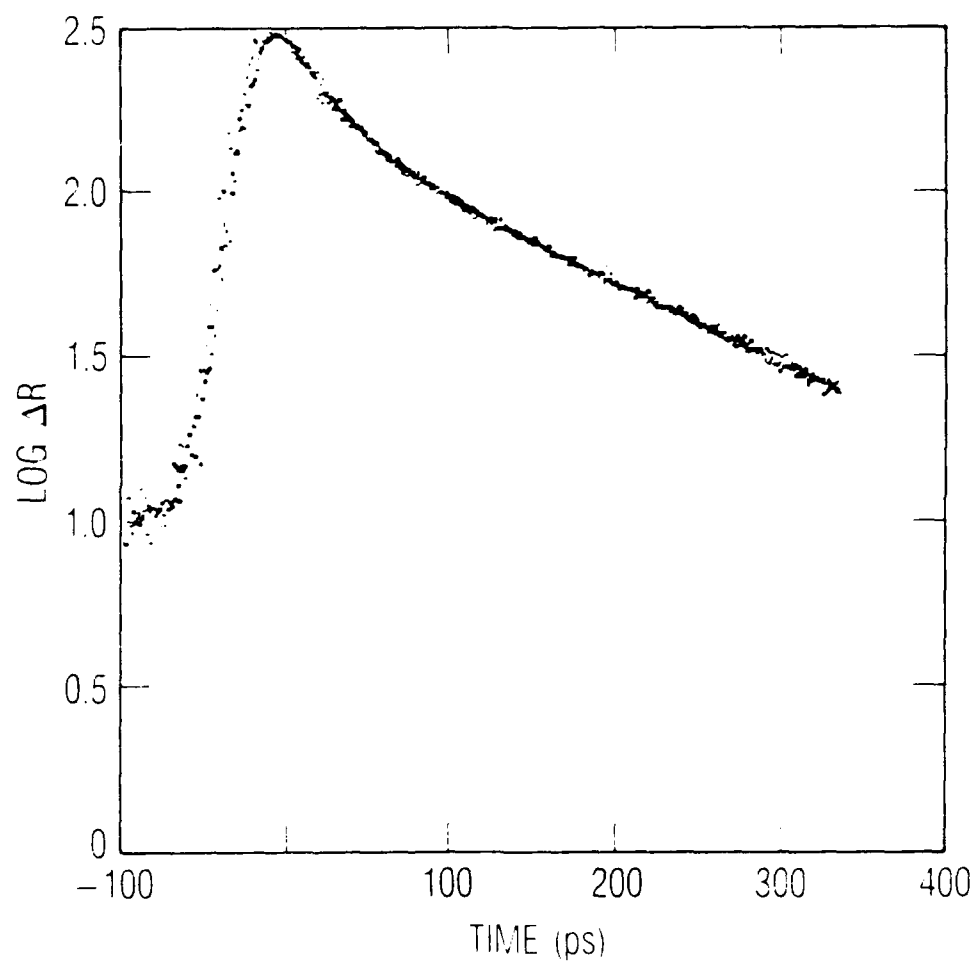


Fig. 2. Picosecond transient reflectivity decay recorded for unwashed n-type GaAs nominally doped with silicon.

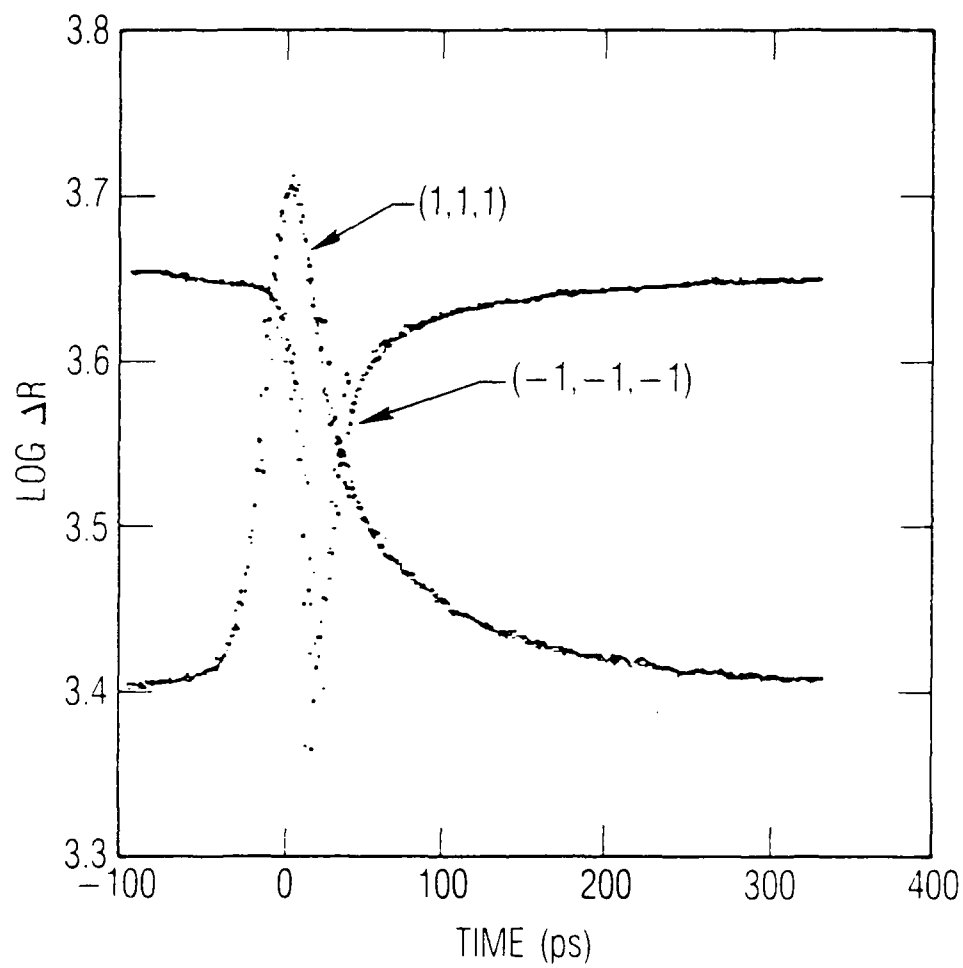


Fig. 3. Picosecond transient reflectivity decays recorded for unwashed (111) and (-1,-1,-1) GaA nominally doped with silicon, same wafer.

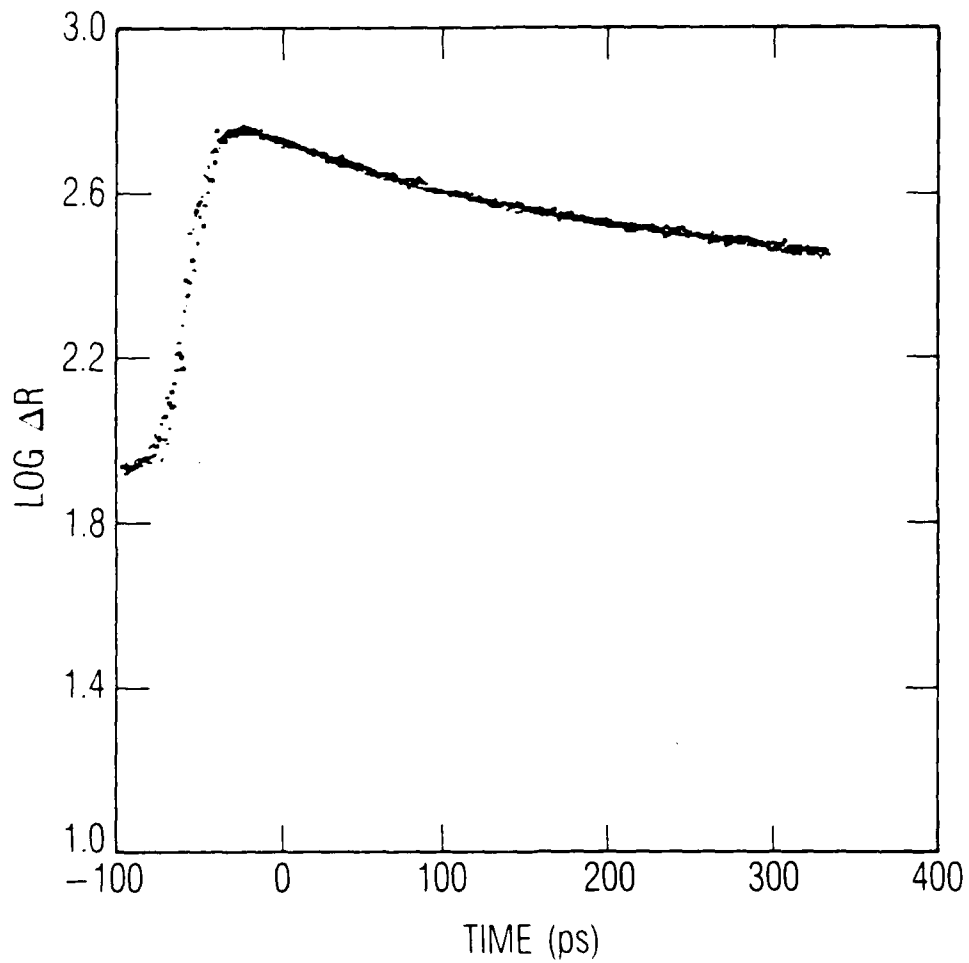


Fig. 4. Picosecond transient reflectivity decay recorded for unwashed p-doped GaAs doped with Zn to $8 \times 10^{18} \text{ cm}^{-3}$.

somewhat slower than the cross correlation time for the two laser pulses, 20 ps, and it was somewhat dependent on the overlap position between probe and pump beams. This condition was relatively poorly controlled; therefore, the appreciable risetimes observed in some signals may derive from diffusion of carriers in the surface plane (which will contribute to risetime, if the beams are not overlapped). Similar behavior was observed for washed material.

The probe beam wavelength was varied in order to investigate mechanisms responsible for transient reflectivity signals. It was not possible to control experimental variables well enough to report quantitative wavelength dependence measurements because laser parameters change significantly each time wavelength is changed. Qualitatively, we observed that the transient reflectivity signals always changed sign as the probe wavelength crossed the room temperature bandgap of GaAs. Signals were of comparable magnitude on either side of the bandgap, and maximum signal amplitude was observed for above-bandgap excitation at the approximate wavelength where maximum exciton contributions are anticipated.

The uniform data obtained for photowashed n-type GaAs motivated analytical modeling of a diffusion recombination mechanism, as reported previously. In this case, flat band conditions are assumed to apply, and ambipolar kinetics are used. The ambipolar carrier density, $N(z,t)$, where z is the dimension normal to the sample surface and t is time, is described by:

$$dN(z,t)/dz = G(z,t) + D \nabla^2 N(z,t) - N(z,t)/\tau_r \quad (1)$$

with the boundary conditions:

$$dN(z,t)/dz|_{z=0} = S * N(0,t)/D \quad (2)$$

$$N(L,t) = 0 \quad (3)$$

Carrier generation is described by G , ambipolar diffusion by D , the bulk recombination time constant by τ_r , the surface recombination velocity by S , and sample thickness by L . The final boundary equation above specifies that light is totally absorbed by the sample.

Hoffman, Jarasiunas, Gerritsen, and Nurmikko⁵ derived the analytical solution, given in Eq. (4), for these conditions. The quantity α is the absorption depth, which can be taken as 10^{-4} cm^{-1} at room temperature for near bandgap pump wavelengths.

$$\begin{aligned}
 N(z,t) = & (N_0/2) \exp(-t/\tau_r) \exp(-z^2/4Dt) \{ (W[\alpha(Dt)^{1/2} \\
 & - (z/2)(Dt)^{1/2}] + W[\alpha(Dt)^{1/2} + (z/2)(Dt)^{1/2}] \\
 & - [2(S/D)/(S/D-\alpha)] \{ W[\alpha(Dt)^{1/2} + (z/2)(Dt)^{1/2}] \\
 & - W[(S/D)(Dt)^{1/2} + (z/2)(Dt)^{1/2}] \} \} \quad (4)
 \end{aligned}$$

$$W(x) = \exp(x^2)(1 - \text{erf}(x)) \quad (5)$$

This model was applied to data for photowashed n-type samples, using the standard value of $12 \text{ cm}^2/\text{s}$ for the parameter D , and assuming a value of 1 ns for an impurity-dominated bulk recombination time, typical for our samples. The constants are assumed to be independent of carrier concentration at the fairly low densities employed in the experiment. Equation (4) was evaluated at the surface, $z = 0$, which was justified above on the basis of primarily surface contributions to the reflected probe beam signal. Furthermore, we assumed that the measured change in reflectivity is linearly related to the carrier density. No provision was made for radial carrier concentration dependences introduced by the Gaussian beam profile. This was justified by the value for D , relative to the beam size, given the time scale of the measurements. Also, the finite pulse durations were not treated, therefore the signal risetime was not modeled.

The calculated decay was fit to the observed decay, shown in Fig. 5, by varying values of S . The fit was excellent for $S = 2.0 \times 10^5 \text{ cm/s}$ and with τ_r adjusted to 0.85 ns . The latter provided a slight improvement in modeling decay for long times. The estimated values did not vary substantially when fitting data from other intrinsic, n-doped, or Cr-doped photowashed samples. The photowashing procedure was varied, and delay times between washing and measurements were varied in order to characterize the surface changes. Maximum reflectivity changes were obtained with a 5-min wash period and with 1

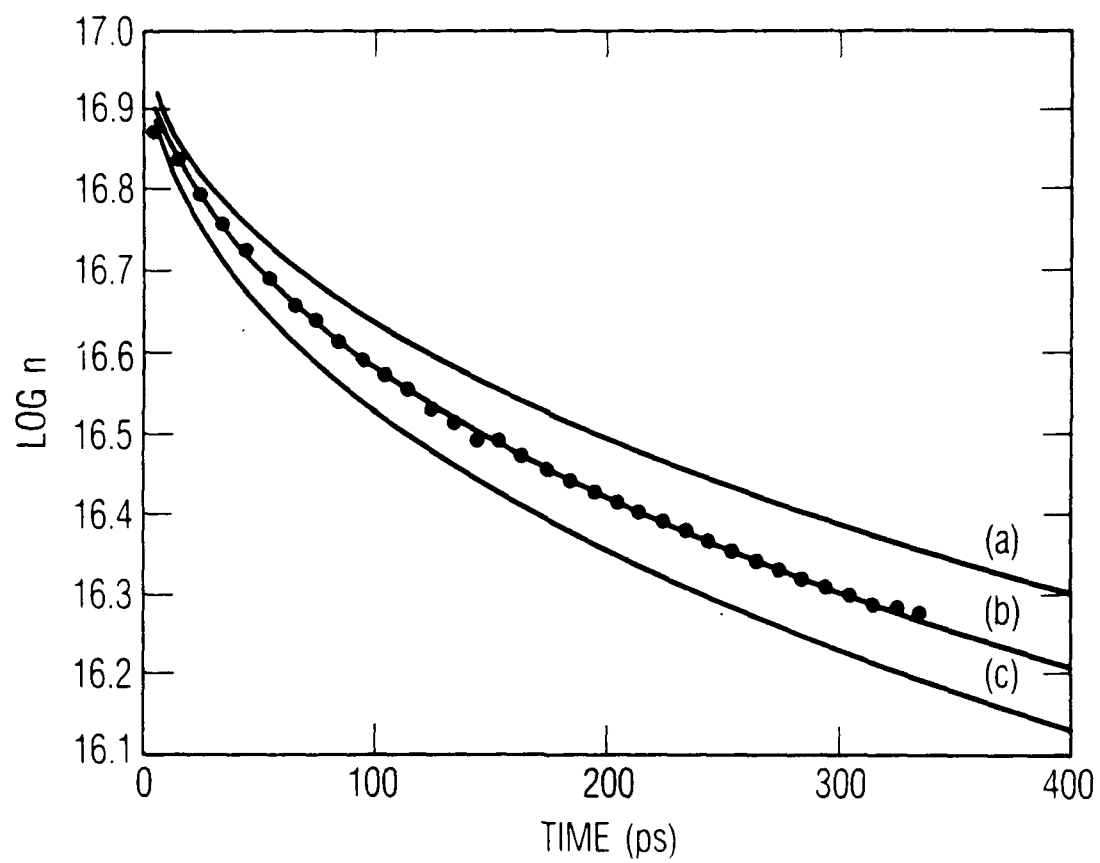


Fig. 5. Picosecond transient reflectivity decay recorded for photowashed GaAs with fit by ambipolar diffusion model.

W/cm² intensity at 514.5 nm. (Measurements were not highly sensitive to these parameters nor to factors such as water flow rate and sample history.) When washing was continued for periods as long as 15 min, signal levels decreased notably. There was also a definite decrease in signals as a function of time following washing, for samples subjected to the nominal 5-min photowashing. Photowashing of other types of samples, such as p-type GaAs and n-type (111) surfaces, led to a larger variation of decay curves from sample to sample. Whereas the ambipolar diffusion model described reflectivity signals from photowashed material precisely, data from unwashed and from normally etched samples deviated greatly from the functional form of Eq. (4). Figure 6 displays one of the best fits to data from an unwashed sample obtained from Eq. (4).

Based on the expectation that unwashed samples have a strong surface electric field, more sophisticated modeling of charge carrier dynamics was required. Computer simulations were performed using a modified version of the Poisson and Continuity Equation Solver (PISCES) computer code from Stanford University. The program includes models for GaAs properties, Fermi-Dirac statistics, a surface charge layer, and processes such as Auger recombination and surface recombination. Optical carrier generation was added to the basic code, and cylindrical coordinates were used in order to take advantage of the cylindrical symmetry of the experiment. Therefore, the simulation is essentially two-dimensional, with a depth position y and a radial position x . Temporal and spatial profiles were chosen to match the experimental conditions. The pulse was assumed to be exponential with a 12-ps time constant, and the beam was assumed to have a Gaussian profile with a 10- μ m radius ($1/e$). The peak injected carrier concentration was selected to be 2×10^{18} cm⁻³, corresponding to 0.2 nJ per pulse. The calculations for unwashed GaAs with internal fields were set up using a surface charge layer chosen to create the desired field. Since PISCES cannot treat surface recombination with boundary conditions for current, an artificial boundary was used. This consisted of specifying a thin oxide layer on top of the GaAs, to enforce a zero current boundary condition, with a zero voltage boundary condition applied to the upper oxide surface. The interface recombination velocity S

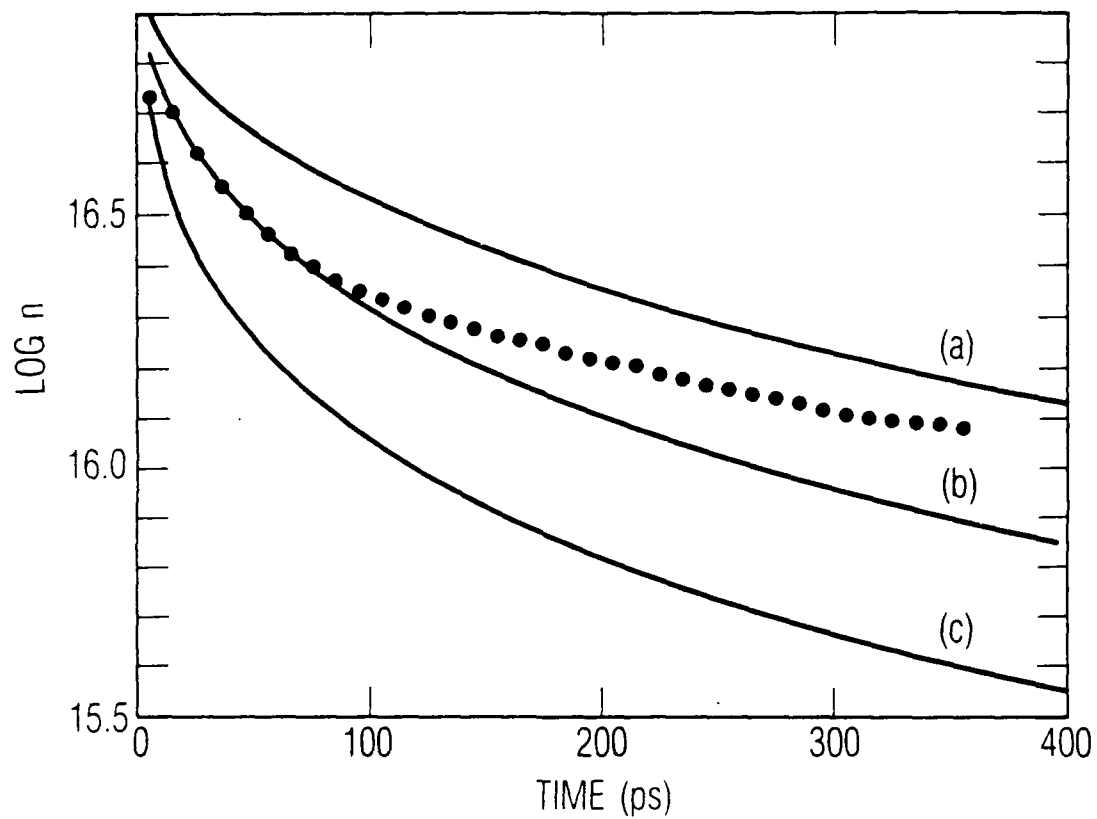


Fig. 6. Comparison of the measured reflectivity decay for typical unwashed n-type GaAs and the best fitting achieved using the ambipolar diffusion model.

and surface charge Q of the oxide are specified as parameters. Multiple simulations were run with different values for S and Q until a good fit to the experimental data was obtained. The output of a simulation consisted of carrier concentrations and the potential at each grid point in the sample. The reflectivity change was assumed to be proportional to the difference between the calculated carrier density and the equilibrium value, which is determined by the surface charge. Under our experimental conditions, the reflectivity signal arises from a surface layer of depth 10^{-6} cm, and since the PISCES carrier density depth profiles vary little over this distance, signals were assumed to be proportional to the surface carrier density, thereby avoiding the need to average over depth.

The PISCES calculation was initially used to model the well understood behavior for washed n-doped GaAs. In this case, the surface charge was set to $Q = 0$ and surface recombination velocity was varied, obtaining a best fit to the data for $S = 4.5 \times 10^5$ cm/s. The fit was equally good for $0 \geq Q \geq -5 \times 10^{11}$ cm $^{-2}$, providing an upper limit to the initial surface charge density. It is interesting to note that the fit was equally good at $Q = 0$ if the change in the reflection signal (ΔR) was taken to be proportional to either the change in the electron or the hole concentration. This is evidence for ambipolar kinetics, consistent with small electric fields at the washed surface. The results of the fit obtained for the cases where ΔR is assumed to be proportional to hole concentration and where ΔR is assumed to be proportional to electron concentration are shown in Figs. 7 and 8, respectively.

PISCES was then applied to fit data obtained from a typical unwashed n-type GaAs sample, with nominal doping about 2×10^{17} /cm 3 . The best calculated results are shown in Fig. 9, where reflectivity change is assumed to correlate with hole density. Surface charge density was $Q = -1.1 \times 10^{12}$ /cm 2 , and surface recombination velocity was $S = 1.3 \times 10^6$ cm/s. The electron density was also modeled, as shown in Fig. 10. In this case, it was necessary to assume a nonphysical ($Q > 0$) value of surface charge, $Q = +3 \times 10^{11}$ /cm 3 in order to fit the data. Although it is difficult to conclusively attribute the observed reflectivity changes to changes in hole concentration, the quality of fit for the hole density is significantly better than that for the electron density.

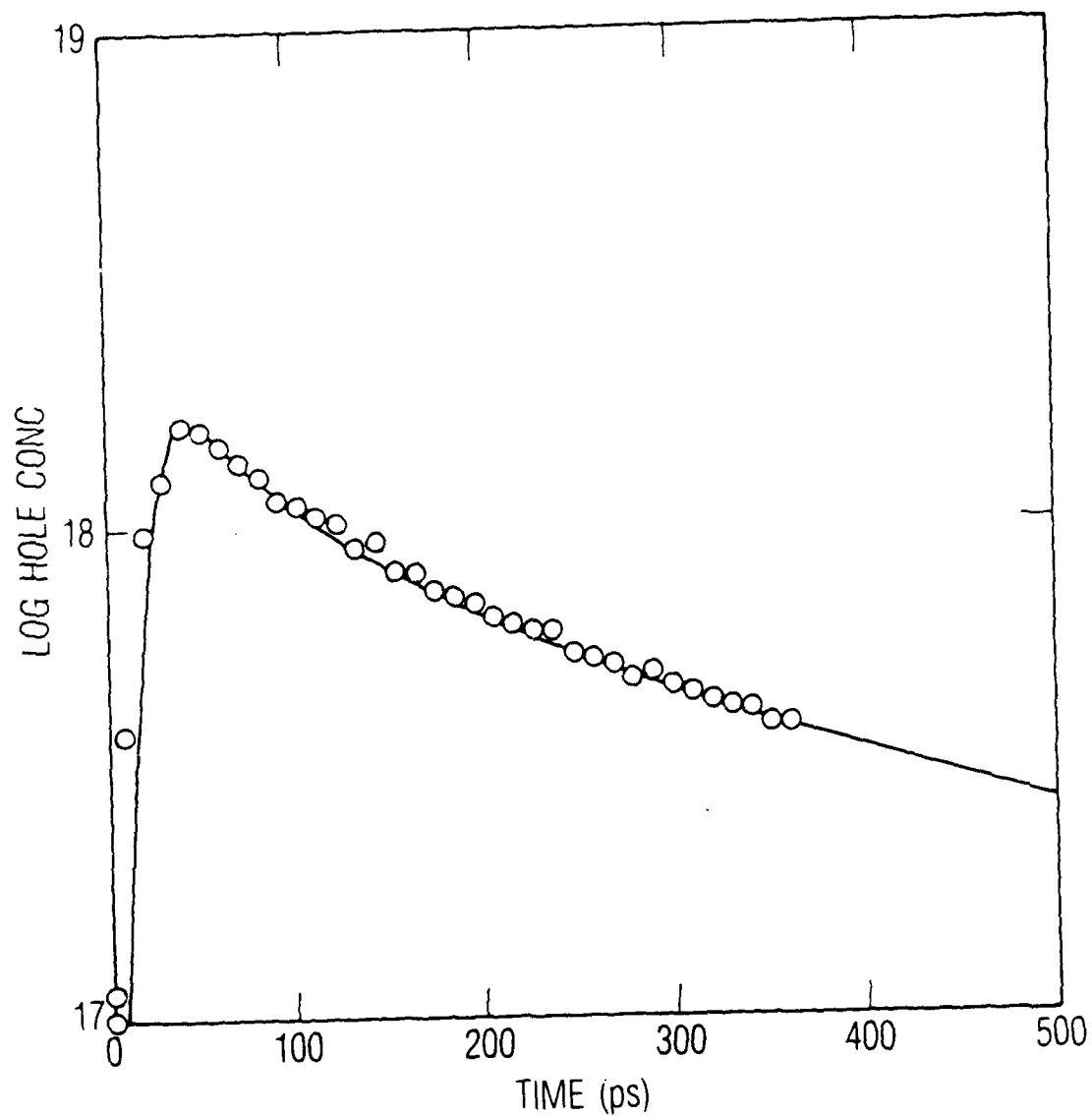


Fig. 7. Calculation of best fit by the PISCES calculation to data for photowashed n-type GaAs, using hole density as the time dependent variable.

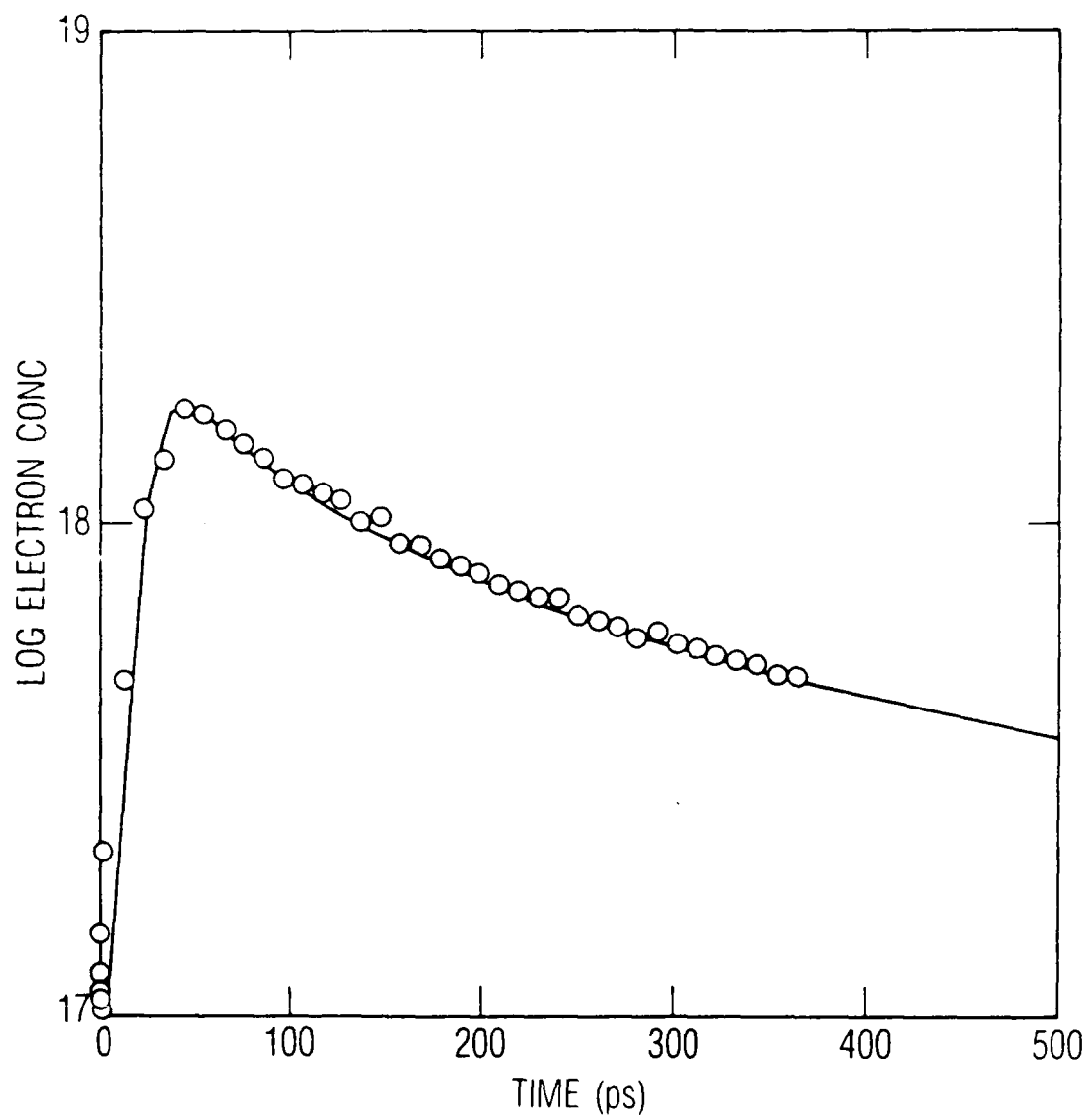


Fig. 8. Time dependence of electron density predicted for positive surface charge is compared with the observed decay from photowashed n-type GaAs.

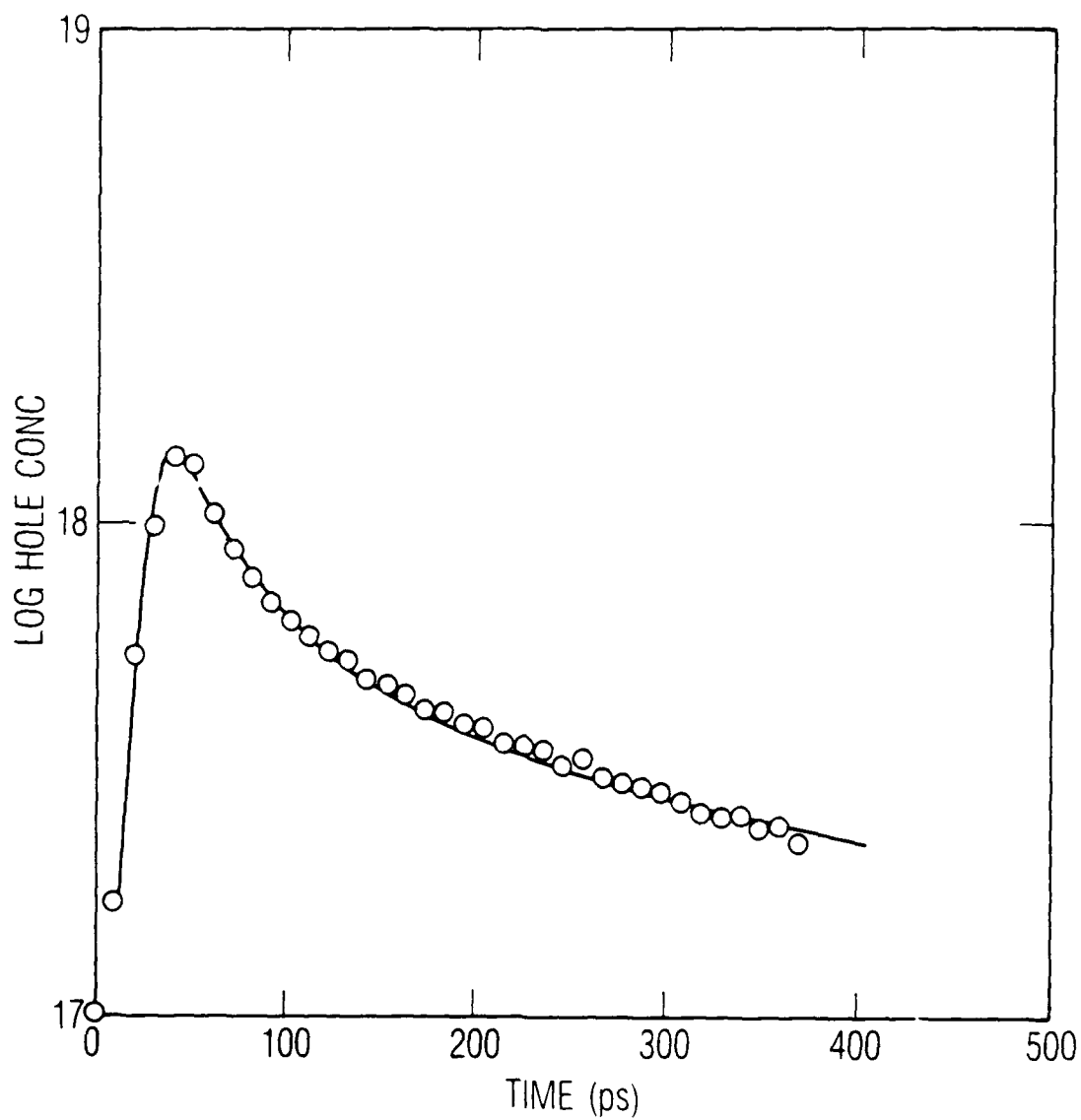


Fig. 9. Predicted time dependence of hole density decay with surface charge and surface recombination velocity adjusted for an optimum fit to data for typical unwashed n-type GaAs.

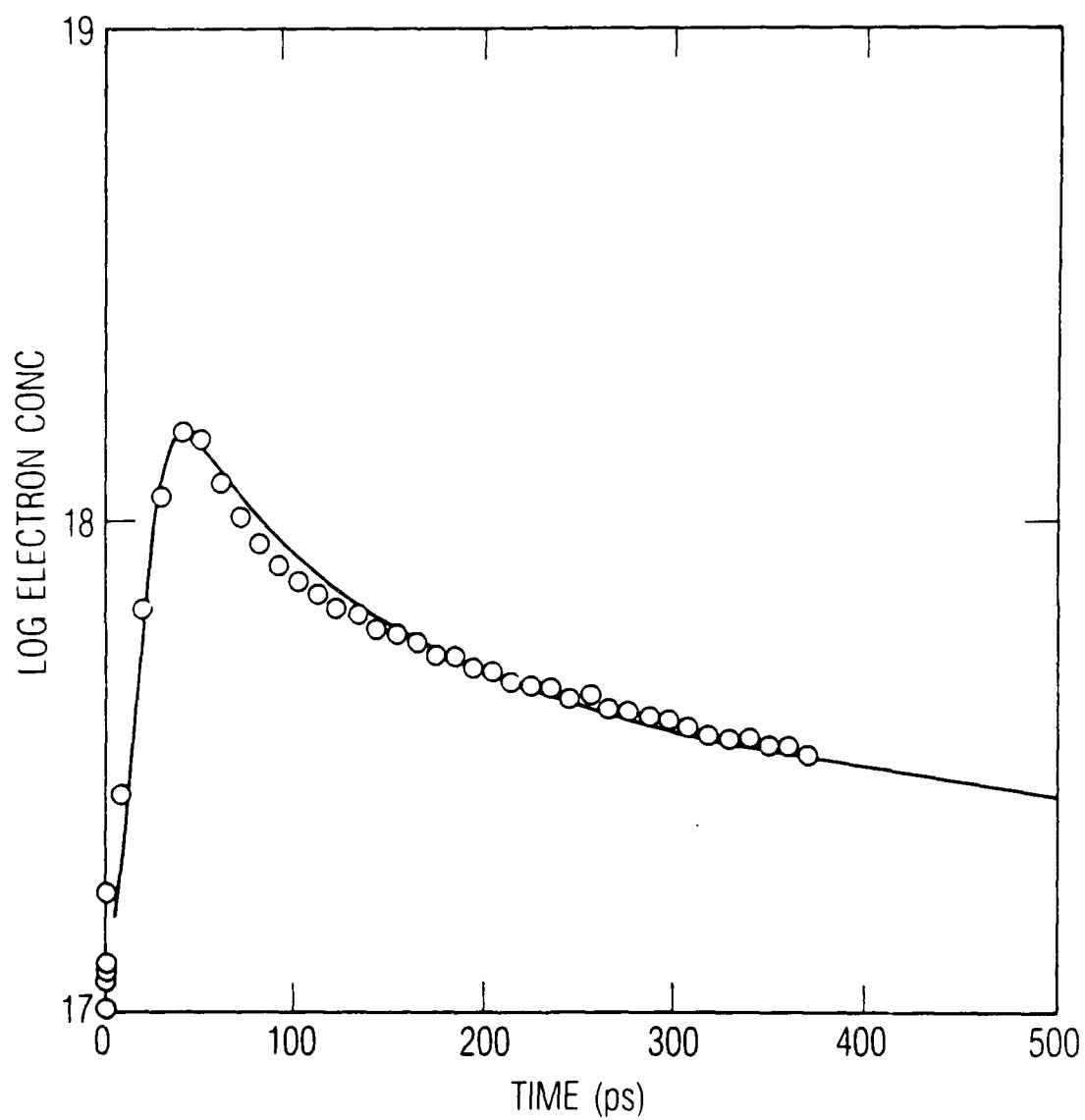


Fig. 10. Predicted time dependence of electron density with surface charge and surface recombination velocity adjusted for an optimum fit to data for typical unwashed n-type GaAs.

IV. DISCUSSION

The picosecond-transient reflectivity technique provides high quality data with signal-to-noise ratios exceeding 100 for a time resolution of about 20 ps. This is possible even though the signals represent small changes, of order 1 part in 10^5 , in the overall probe beam intensity. High-frequency modulation techniques greatly facilitate the measurements. The major advantage of the approach, versus the more widely used picosecond transient-grating method, is that the former is relatively insensitive to surface diffusion, whereas the grating method is highly sensitive to diffusion in this dimension. Surface diffusion is not of direct concern in our recombination studies, therefore the reflection technique is highly advantageous. However, as mentioned in section III, surface diffusion effects are manifested as an artifact in the reflectivity data if the probe beam position is offset from that of the pump. The overlap dependence could be used to follow fast movement of excitations, such as surface plasmons or polaritons, which would diffuse macroscopic distances on a picosecond time scale.

One of the more interesting questions posed by these studies concerns the physical mechanism responsible for reflectivity changes on the picosecond time scale. A number of prior studies address aspects of this problem. None provide a firm basis for assessing conditions applicable to our experiments. In several studies involving picosecond excitation of semiconductors^{10,11}, a Drude mechanism has been invoked to predict reflectivity changes subsequent to charge injection. This mechanism is important at long wavelengths and for large carrier densities. It may contribute under our conditions. However, the observed wavelength dependence of signal phase is inconsistent with substantial Drude contributions. The same observation rules out contributions from intervalence absorption, which has also been suggested⁹ as a mechanism responsible for reflectivity changes.

The studies¹² of Lee et al. are the most relevant to our experimental conditions, even though their treatment was limited to the case of CW excitation, with monitoring by absorption. Given intensities comparable to

the time-average intensities employed here, they identify three nonlinear contributions. Exciton bleaching is prominent, leading to a dispersive change in refractive index near the bandgap. A smaller dispersive contribution comes from band filling. Even at the low intensities reported, there is a significant effect from bandgap renormalization. Lee and coworkers performed calculations that identified these separate contributions, and the combined results were fitted to experimental measurements. We lack the quantitative data for such modeling. On a qualitative basis, our data show a 180° phase reversal in the signals as probe wavelength crosses the E_0 bandgap. This is consistent with the exciton bleaching and band filling mechanisms and with the Franz-Keldysh mechanism. In the latter case, additional oscillations of signal phase should also be observed above bandgap. Under our experimental conditions, there should be strong screening of the effective surface field shortly after excitation. This should suppress the Franz-Keldysh reflectivity oscillations expected for the unpumped material. Therefore the full Franz-Keldysh effect associated with the surface field could be expected to appear in the data. We estimate that this should contribute a signal with modulation depth in the range 10^{-5} to 10^{-4} , which is consistent with observations. One interesting test of this mechanism will be to compare wavelength dependence results for washed and unwashed GaAs. Since the washed surface is presumably free from surface fields, the Franz-Keldysh contribution to signals should vanish. The exciton bleaching mechanism could result in comparable-magnitude reflectivity signals, but it would not display above bandgap oscillations. Currently, experiments are under way to differentiate between these mechanisms.

Picosecond transient reflectivity provides an indirect probe of chemistry at the sample surface, as deduced from changes in charge carrier dynamics. The large diversity of signals observed for GaAs from different sources and its high sensitivity to surface processing suggest that extensive chemistry occurs at the surface. This has been discussed extensively by others. Our results, namely, that fast, complex decay of surface excitation is observed for mechanically polished material, for materials as received from crystal growers, and from samples subjected to some common etching procedures, are

generally consistent with the most recent findings by others. It was previously suggested⁷ that for n-type (100) material, a substantial deposit of arsenic and gallium oxides and arsenic metal form on the surface. These materials contribute midgap states that are filled by carriers and result in strong band bending. Arsenic oxide is relatively water soluble, therefore washing is expected to be an effective means for removal. Arsenic metal can be oxidized by oxygenated water in the presence of photons, and photons may assist in solvation of gallium oxides. The gallium oxides are relatively insoluble; therefore, prolonged washing simply results in buildup of an excessively thick layer of this material. This may explain the reappearance of band bending with prolonged washing.

The major differences between signals observed for opposite polar surfaces and the lack of similarity between signals from p-type material and that for the other materials suggests that the surface states, and possibly surface chemistry, differ between these types of surfaces. We intend to investigate these differences using the PISCES model in the future. It will also be interesting to study the relationship between the picosecond reflectivity results and the slower time scale results obtained by conventional photorefectivity methods². Reflectivity changes measured by the conventional method are attributed to the Franz-Keldysh mechanism. Some groups report¹² that photowashing does not eliminate surface pinning associated with the slow surface traps that are measured by this conventional method. The differences between these observations and those made in the picosecond experiments may be attributed to the different measurement conditions. Low intensity sources are employed in conventional reflection spectroscopy, such that injected carriers weakly perturb the surface potential. In contrast, the picosecond technique injects about 10^{14} carriers/cm², vastly exceeding the initial surface charge density. Thus, an initial fast screening occurs, followed by a transient regime of effectively reduced surface field. The rapid recombination at the surface then depletes screening charge near the surface, and a short-range field builds up. These effects are implicit to the PISCES calculation; therefore, it correctly models decay kinetics on the fast time scale. No provision has been made to treat

the more complex slow processes that may occur. In the future, it may be practical to modify the artificial surface insulator layer incorporated in the PISCES model, thereby providing a unified model capable of treating both fast and slow processes. With current experimental techniques in which pulses are repeated each 4 ns, charge may build up in slow states, due to prior pump pulses, thereby screening these states. It would be desirable to perform measurements with individual low-intensity pulses, such that no charge accumulates from prior pulses, thus avoiding the problem.

V. CONCLUSION

Prior studies clearly established that photowashing procedures significantly reduce surface recombination in GaAs. Modeling of picosecond transient-reflectivity data demonstrated that, for times from 20 to 400 ps, charge carrier transport within 10^{-4} cm of the surface occurs under essentially flat band conditions for washed n-type, Cr-doped, and intrinsic material. The same technique identifies strong band bending for unwashed surfaces.

Results from modeling charge-transport in the presence of strong band bending using the PISCES computer code were highly successful. The most typical reflectivity decay curves obtained from unwashed material, which could not be described by the analytical ambipolar kinetics model, were fit exceedingly well by the PISCES calculation, using physically reasonable values for the variables. The optimum surface charge density, $Q = -10^{12}/\text{cm}^2$, is consistent with that estimated by other techniques, and the optimum value for surface recombination velocity of $S = 10^6$ cm/s, is also within ranges reported by other techniques. This provides good support for the validity of the model and suggests that it can be used for quantitative characterization of surface conditions. Clearly, a number of fundamental issues remain unresolved, including the physical origin of the transient reflectivity signal on picosecond time scales, and the differences in behavior between the picosecond regime and prior studies on slower time scales.

REFERENCES

1. W. E. Spicer, I. Lindau, P. Skeath, C. Y. Su, and P. Chye, J. Vac. Sci. Tech. **17**, 1019 (1980); J. M. Woodall and J. L. Freeour, J. Vac. Sci. Tech. **19**, 794 (1981).
2. O. J. Glembocki, B. V. Shanabrook, N. Bottka, W. T. Beard, and J. Comas, in Proc. SPIE, Spectroscopic Characterization Techniques for Semiconductor Technology II, Vol. 524, ed. F. H. Pollack (1985) pg. 86.
3. S. M. Beck and J. E. Wessel, Appl. Phys. Lett. **50**, 149 (1987).
4. Poisson and Continuity Equation Solver (PISCES II B), Stanford Electronics Laboratories, Dept. of Electrical Engineering, Stanford University.
5. C. A. Hoffman, K. Jarasiunas, H. J. Gerritsen, and A. V. Nurmikko, Appl. Phys. Lett. **33**, 536 (1978).
6. D. G. McLean, M. G. Roe, A. I. D'Souza, and P. E. Wigen, Appl. Phys. Lett. **48**, 992 (1986).
7. S. D. Offsey, J. M. Woodall, A. C. Warren, P. D. Kirchnen, T. I. Chappell, and G. D. Pettit, Appl. Phys. Lett. **48**, 475 (1986).
8. N. A. Ives, G. Stupian, and M. S. Leung, Appl. Phys. Lett. **50**, 256 (1987).
9. D. E. Aspnes and A. Frova, Solid State Commun. **7**, 155 (1969).
10. C. V. Shank, R. Yen, and C. Hirlimann, Phys. Rev. Lett. **50**, 454 (1983); **51**, 900 (1983).
11. R. Yen, S. M. Liu, H. Kurz, and N. Bloembergen, Appl. Phys. **A27**, 153 (1982).
12. Y. H. Lee, A. Chavez-Pirson, S. W. Koch, H. M. Gibbs, S. H. Park, J. Morhange, A. Jeffery, N. Peyghambarian, L. Banyai, A. C. Gossard, and W. Wiegmann, Phys. Rev. Lett. **57**, 2446 (1986).
13. K. Gaskill, Naval Research Laboratory, private communication.

LABORATORY OPERATIONS

The Aerospace Corporation functions as an "architect-engineer" for national security projects, specializing in advanced military space systems. Providing research support, the corporation's Laboratory Operations conducts experimental and theoretical investigations that focus on the application of scientific and technical advances to such systems. Vital to the success of these investigations is the technical staff's wide-ranging expertise and its ability to stay current with new developments. This expertise is enhanced by a research program aimed at dealing with the many problems associated with rapidly evolving space systems. Contributing their capabilities to the research effort are these individual laboratories:

Aerophysics Laboratory: Launch vehicle and reentry fluid mechanics, heat transfer and flight dynamics; chemical and electric propulsion, propellant chemistry, chemical dynamics, environmental chemistry, trace detection; spacecraft structural mechanics, contamination, thermal and structural control; high temperature thermomechanics, gas kinetics and radiation; cw and pulsed chemical and excimer laser development including chemical kinetics, spectroscopy, optical resonators, beam control, atmospheric propagation, laser effects and countermeasures.

Chemistry and Physics Laboratory: Atmospheric chemical reactions, atmospheric optics, light scattering, state-specific chemical reactions and radiative signatures of missile plumes, sensor out-of-field-of-view rejection, applied laser spectroscopy, laser chemistry, laser optoelectronics, solar cell physics, battery electrochemistry, space vacuum and radiation effects on materials, lubrication and surface phenomena, thermionic emission, photo-sensitive materials and detectors, atomic frequency standards, and environmental chemistry.

Computer Science Laboratory: Program verification, program translation, performance-sensitive system design, distributed architectures for spaceborne computers, fault-tolerant computer systems, artificial intelligence, micro-electronics applications, communication protocols, and computer security.

Electronics Research Laboratory: Microelectronics, solid-state device physics, compound semiconductors, radiation hardening; electro-optics, quantum electronics, solid-state lasers, optical propagation and communications; microwave semiconductor devices, microwave/millimeter wave measurements, diagnostics and radiometry, microwave/millimeter wave thermionic devices; atomic time and frequency standards; antennas, rf systems, electromagnetic propagation phenomena, space communication systems.

Materials Sciences Laboratory: Development of new materials: metals, alloys, ceramics, polymers and their composites, and new forms of carbon; non-destructive evaluation, component failure analysis and reliability; fracture mechanics and stress corrosion; analysis and evaluation of materials at cryogenic and elevated temperatures as well as in space and enemy-induced environments.

Space Sciences Laboratory: Magnetospheric, auroral and cosmic ray physics, wave-particle interactions, magnetospheric plasma waves; atmospheric and ionospheric physics, density and composition of the upper atmosphere, remote sensing using atmospheric radiation; solar physics, infrared astronomy, infrared signature analysis; effects of solar activity, magnetic storms and nuclear explosions on the earth's atmosphere, ionosphere and magnetosphere; effects of electromagnetic and particulate radiations on space systems; space instrumentation.